



ELSEVIER

Available online at www.sciencedirect.com

SCIENCE @ DIRECT®

Journal of Sound and Vibration 283 (2005) 665–683

JOURNAL OF
SOUND AND
VIBRATION

www.elsevier.com/locate/jsvi

Transverse vibration analysis and measurement for the piezoceramic annular plate with different boundary conditions

Chi-Hung Huang

Department of Mechanical Engineering, Ching Yun University, Chien-Hsin Rd. 229, Chung-Li 320, Taiwan

Received 2 December 2003; received in revised form 23 April 2004; accepted 5 May 2004

Available online 15 December 2004

Abstract

Through means of the electroelastic theory for piezoelectric plates, the transverse vibration characteristics of piezoceramic annular plates with different boundary conditions are investigated in this work by theoretical analysis, numerical simulation and experimental verification. There are four different boundary conditions (free–free, fixed–fixed, free–fixed, and fixed–free) to be considered herein. With the aid of theoretical analysis, three groups of vibration modes are defined and employed for making the mode classification. Combined with the mode shape recognition, the classification is valid for the prediction of resonant frequency variations with various boundary conditions. Two experimental methods, laser Doppler vibrometer (LDV) and impedance analyzer, are applied to validate the theoretical results for the free–free boundary condition. From the experimental results, we find that the transverse vibration modes cannot be measured by the impedance analysis and only the extensional vibration modes will be shown. However, the transverse vibration modes of piezoceramic annular plates are obtained by the LDV system.

© 2004 Elsevier Ltd. All rights reserved.

1. Introduction

Because of the high electromechanical performance, the piezoelectric material is widely used in many applications, such as ultrasonic transducers, actuators, sensors, electro-optic modulators, and so on. Piezoelectricity describes the phenomenon in which the material generates electric charge when subjected to stress and, conversely, generates strain when the electric field is applied.

E-mail address: chhuang@cyu.edu.tw (C.-H. Huang).

0022-460X/\$ - see front matter © 2004 Elsevier Ltd. All rights reserved.

doi:10.1016/j.jsv.2004.05.034

According to the different configurations, the piezoceramic transducers possess many vibration modes in various application fields. In general, there are three principal vibration modes of transducers; the extensional modes of thin piezoceramic circular or annular plates, the tangential modes of thin piezoceramic rectangular plates, and the longitudinal modes of slender piezoceramic cylinders; which had been addressed in many studies. Especially for piezoceramics made of lead zirconate titanate (PZT), numerous investigations have been performed on the disk or annulus types in the analysis and application, e.g. Langevin transducers and ultrasonic motors. To maximize the dynamic electromechanical coupling coefficient, Ivina [1] used the finite element method to study the symmetric modes of vibration for circular piezoelectric plates in determining the resonant and anti-resonant frequencies, radial mode configurations, and the optimum geometrical dimensions. Kunkel et al. [2] studied the vibration modes of PZT-5H ceramics disks concerning the diameter-to-thickness (D/T) ratio ranging from 0.2 to 10. Guo et al. [3] presented the results for PZT-5A piezoelectric disks with D/T of 20 and 10. In that study, there were five types of modes classified according to the mode shape characteristics, and the physical interpretation was clarified. Iula et al. [4] proposed a matrix model of the radial symmetric mode of a thin piezoceramic ring while the inner and outer lateral surfaces are loaded by the surrounding medium. The resonant frequency spectrum and effective electromechanical coupling coefficient (k_{eff}) are discussed as functions of the inner-to-outer radius ratio. Furthermore, by using the previously proposed model, Iula et al. [5] defined the material coupling factor (k_{mat}) for the ring geometry to take into account its variation with respect to the inner-to-outer radius ratio. Shuyu [6] found that the thickness shearing vibration of the tangential polarized piezoceramic ring is related to the cross-sectional shape and dimension. By theoretical and experimental investigations, the effect of the cross-sectional shape factor on the electromechanical coupling coefficient and resonant frequency had been verified. Takano et al. [7] employed the in-plane non-axisymmetric vibration modes of a piezoelectric annular plate to investigate the application on an ultrasonic motor. In use of the analysis of displacement and electromechanical coupling factor, the favorable vibration modes are suggested for different ultrasonic motor configurations. Wang et al. [8] employed the Kirchhoff plate model and quadratic potential function to investigate the free vibration of a piezoelectric coupled circular plate. The theoretical model was verified by comparing with the finite-element analysis.

Most of the research and applications about piezoceramic annular plates had been carried out more on the extensional vibrations and less on the transverse vibrations. According to the theory for piezoelectricity and Kirchhoff–Love plate hypotheses, the transverse vibration modes of piezoceramic annular plates with four different boundary conditions (free–free, fixed–fixed, free–fixed, and fixed–free) are investigated. The theoretical analysis presented in this paper can be taken as special cases of the article by Wang et al. [8]. To validate the theoretical results, this study utilizes two optical techniques, laser Doppler vibrometer (LDV), and the electrical impedance analyzer for measuring the vibration properties of piezoceramic annular plates with the free–free boundary condition. According to the experimental results, only the extensional vibration modes are measured by the impedance analysis and the transverse vibration modes can be verified by the LDV system [9]. Commercially available finite element analysis is also used to provide the numerical solutions and evidences. To understand the influence on the inner-to-outer radius ratio, the variations in resonant frequencies are calculated and classified into three groups for the different boundary conditions in the work.

2. Theoretical analysis for the piezoceramic annular plate

The vibration of piezoelectric material is electroelastic in nature, and it is necessary to include the coupled electrical field with the elastic behavior. In other words, the equations of linear elasticity are coupled to the charge equation of electrostatics by means of the piezoelectric constants. The system of governing equations, in cylindrical coordinates, needed to determine the vibration characteristics of piezoelectric materials are presented as follows [10–12]:

The differential equations of equilibrium are

$$\frac{\partial \sigma_{rr}}{\partial r} + \frac{1}{r} \frac{\partial \sigma_{r\theta}}{\partial \theta} + \frac{\partial \sigma_{rz}}{\partial z} + \frac{1}{r} (\sigma_{rr} - \sigma_{\theta\theta}) + \rho \frac{\partial^2 u}{\partial t^2} = 0, \tag{1a}$$

$$\frac{\partial \sigma_{r\theta}}{\partial r} + \frac{1}{r} \frac{\partial \sigma_{\theta\theta}}{\partial \theta} + \frac{\partial \sigma_{\theta z}}{\partial z} + \frac{2}{r} \sigma_{r\theta} + \rho \frac{\partial^2 v}{\partial t^2} = 0, \tag{1b}$$

$$\frac{\partial \sigma_{rz}}{\partial r} + \frac{1}{r} \frac{\partial \sigma_{\theta z}}{\partial \theta} + \frac{\partial \sigma_{zz}}{\partial z} + \frac{1}{r} \sigma_{rz} + \rho \frac{\partial^2 w}{\partial t^2} = 0, \tag{1c}$$

where $\sigma_{rr}, \sigma_{r\theta}, \dots, \sigma_{zz}$ are the components of stress; u, v and w are the displacement field in the r, θ and z direction, respectively; and ρ is the density.

The strain–mechanical displacement relations are

$$\begin{aligned} e_{rr} &= \frac{\partial u}{\partial r}, & e_{\theta\theta} &= \frac{u}{r} + \frac{1}{r} \frac{\partial v}{\partial \theta}, \\ e_{zz} &= \frac{\partial w}{\partial z}, & e_{r\theta} &= \frac{1}{r} \frac{\partial u}{\partial \theta} + \frac{\partial v}{\partial r} - \frac{v}{r}, \\ e_{rz} &= \frac{\partial u}{\partial z} + \frac{\partial w}{\partial r}, & e_{\theta z} &= \frac{\partial v}{\partial z} + \frac{1}{r} \frac{\partial w}{\partial \theta}, \end{aligned} \tag{2}$$

where $e_{rr}, e_{r\theta}, \dots, e_{zz}$ are the components of strain.

The linear piezoelectric constitutive equations for piezoceramic materials are

$$\begin{bmatrix} e_{rr} \\ e_{\theta\theta} \\ e_{zz} \\ e_{\theta z} \\ e_{rz} \\ e_{r\theta} \\ D_r \\ D_\theta \\ D_z \end{bmatrix} = \begin{bmatrix} s_{11}^E & s_{12}^E & s_{13}^E & 0 & 0 & 0 & 0 & 0 & d_{31} \\ s_{12}^E & s_{11}^E & s_{13}^E & 0 & 0 & 0 & 0 & 0 & d_{31} \\ s_{13}^E & s_{13}^E & s_{33}^E & 0 & 0 & 0 & 0 & 0 & d_{33} \\ 0 & 0 & 0 & s_{44}^E & 0 & 0 & 0 & d_{15} & 0 \\ 0 & 0 & 0 & 0 & s_{44}^E & 0 & d_{15} & 0 & 0 \\ 0 & 0 & 0 & 0 & 0 & s_{66}^E & 0 & 0 & 0 \\ 0 & 0 & 0 & 0 & d_{15} & 0 & \varepsilon_{11}^T & 0 & 0 \\ 0 & 0 & 0 & d_{15} & 0 & 0 & 0 & \varepsilon_{11}^T & 0 \\ d_{31} & d_{31} & d_{33} & 0 & 0 & 0 & 0 & 0 & \varepsilon_{33}^T \end{bmatrix} \begin{bmatrix} \sigma_{rr} \\ \sigma_{\theta\theta} \\ \sigma_{zz} \\ \sigma_{\theta z} \\ \sigma_{rz} \\ \sigma_{r\theta} \\ E_r \\ E_\theta \\ E_z \end{bmatrix}, \tag{3}$$

where $s_{11}^E, s_{12}^E, \dots, s_{66}^E$ are the compliance constants; d_{15}, d_{31}, d_{33} are the piezoelectric constants; $\varepsilon_{11}^T, \varepsilon_{33}^T$ are the dielectric constants; D_r, D_θ, D_z are the electrical displacements, and E_r, E_θ, E_z are the electrical fields.

The charge equations of electrostatics are

$$\frac{\partial D_r}{\partial r} + \frac{1}{r} \frac{\partial D_\theta}{\partial \theta} + \frac{1}{r} D_r + \frac{\partial D_z}{\partial z} = 0. \quad (4)$$

The electric field–electric potential relations are

$$E_r = -\frac{\partial \varphi}{\partial r}, \quad E_\theta = -\frac{1}{r} \frac{\partial \varphi}{\partial \theta}, \quad E_z = -\frac{\partial \varphi}{\partial z}, \quad (5)$$

where φ is the electrical potential.

To simplify the derivation for piezoceramic plates, the following basic hypotheses, including the Kirchhoff–Love plate theory, are employed in the analysis.

- (a) Normal stress σ_{zz} can be neglected relative to the principal stresses, i.e. $\sigma_{zz} = 0$.
- (b) The rectilinear element normal to the middle surface before deformation remains perpendicular to the strained surface after deformation and the elongation of which can be neglected, i.e. $e_{rz} = e_{\theta z} = 0$.
- (c) Electrical potential varies with the thickness by the square law, i.e. $\varphi = \varphi_0 + z\varphi_1 + z^2\varphi_2$; where φ_0, φ_1 and φ_2 are constants.
- (d) Electrical displacement D_z is a constant with respect to plate thickness.

According to hypotheses (a) and (b), the electroelasticity relation of Eq. (3) can be simplified as

$$\sigma_{rr} = \frac{1}{s_{11}^E(1 - \nu_p^2)} (e_{rr} + \nu_p e_{\theta\theta}) - \frac{d_{31}}{s_{11}^E(1 - \nu_p)} E_z, \quad (6a)$$

$$\sigma_{\theta\theta} = \frac{1}{s_{11}^E(1 - \nu_p^2)} (e_{\theta\theta} + \nu_p e_{rr}) - \frac{d_{31}}{s_{11}^E(1 - \nu_p)} E_z, \quad (6b)$$

$$\sigma_{r\theta} = \frac{1}{s_{66}^E} e_{r\theta} = \frac{e_{r\theta}}{2s_{11}^E(1 + \nu_p)}, \quad (6c)$$

$$D_z = d_{31}(\sigma_{rr} + \sigma_{\theta\theta}) + \varepsilon_{33}^T E_z \quad (6d)$$

in which

$$e_{rr} = \frac{\partial u_r}{\partial r} + z \frac{\partial^2 w}{\partial r^2}, \quad (7a)$$

$$e_{\theta\theta} = \frac{u_r}{r} + \frac{1}{r} \frac{\partial v_\theta}{\partial \theta} + \frac{z}{r} \left[\frac{\partial w}{\partial r} + \frac{\partial}{\partial \theta} \left(\frac{1}{r} \frac{\partial w}{\partial \theta} \right) \right], \quad (7b)$$

$$e_{r\theta} = \frac{1}{r} \frac{\partial u_r}{\partial \theta} + \frac{z}{r} \frac{\partial^2 w}{\partial r \partial \theta} + \frac{\partial v_\theta}{\partial r} + z \frac{\partial}{\partial r} \left(\frac{1}{r} \frac{\partial w}{\partial \theta} \right) - \frac{v_\theta}{r} - \frac{z}{r^2} \frac{\partial w}{\partial \theta} \quad (7c)$$

and the planar Poisson's ratio $\nu_p = -s_{12}^E/s_{11}^E$. It is noted that $u_r = u|_{z=0}$ and $v_\theta = v|_{z=0}$ represent the radial and the tangential displacements of the middle plane, respectively.

Fig. 1 shows the piezoceramic annular plate with external radius R_o , internal radius R_i , and thickness h ; the cylindrical coordinates (r, θ, z) with the origin in the center of the annulus are

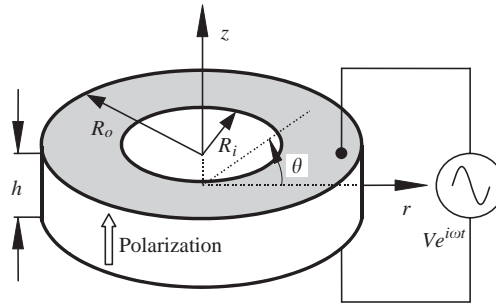


Fig. 1. Geometry and coordinate system of the piezoceramic annular plate.

employed. The piezoceramic annular plate is polarized in the thickness direction and two opposite faces of which are covered with complete electrodes. Since the piezoceramic annular plate is thin, the out-of-plane (transverse) vibration and the in-plane (tangential and extensional) vibration are assumed to decouple. We will analyze in detail the dynamic characteristics for transverse vibrations with different boundary conditions as follows.

Suppose that the piezoceramic annular plate is driven by an AC voltage $Ve^{i\omega t}$ and the transverse vibration is non-axisymmetric, the displacement in the z -direction can be assumed to have the following form:

$$w(r, \theta, t) = W(r, \theta)e^{i\omega t}, \tag{8}$$

where ω is the angular frequency. If the time-dependent term $e^{i\omega t}$ is uniformly suppressed in the analysis, by substituting Eq. (8) into Eqs. (7a)–(7c), then Eqs. (6a)–(6c) of the stress components can be expressed as

$$\sigma_{rr} = \frac{1}{s_{11}^E(1 - \nu_p^2)} \left[z \frac{\partial^2 W}{\partial r^2} + \nu_p \frac{z}{r} \left(\frac{\partial W}{\partial r} + \frac{1}{r} \frac{\partial^2 W}{\partial \theta^2} \right) \right] - \frac{d_{31}}{s_{11}^E(1 - \nu_p)} E_z, \tag{9a}$$

$$\sigma_{\theta\theta} = \frac{1}{s_{11}^E(1 - \nu_p^2)} \left[\frac{z}{r} \left(\frac{\partial W}{\partial r} + \frac{1}{r} \frac{\partial^2 W}{\partial \theta^2} \right) + \nu_p z \frac{\partial^2 W}{\partial r^2} \right] - \frac{d_{31}}{s_{11}^E(1 - \nu_p)} E_z, \tag{9b}$$

$$\sigma_{r\theta} = \frac{1}{s_{11}^E(1 + \nu_p)} \left[\frac{z}{r} \frac{\partial^2 W}{\partial r \partial \theta} - \frac{z}{r^2} \frac{\partial W}{\partial \theta} \right]. \tag{9c}$$

Herein it is assumed that the stresses as above are induced by the out-of-plane displacement $W(r, \theta)$ only. For the electrical potential boundary condition

$$\phi|_{z=\pm \frac{h}{2}} = \pm V \tag{10}$$

we can find that the electrical field is, by combining Eqs. (10), (9a) and (9b),

$$E_z = -\frac{2V}{h} - \frac{d_{31}}{\epsilon_{33}^T} \frac{z}{s_{11}^E(1 - \nu_p)(1 - k_p^2)} \left[\frac{\partial^2 W}{\partial r^2} + \frac{1}{r} \left(\frac{\partial W}{\partial r} + \frac{1}{r} \frac{\partial^2 W}{\partial \theta^2} \right) \right], \tag{11}$$

where $k_p = \sqrt{2d_{31}^2/\epsilon_{33}^T s_{11}^E(1 - \nu_p)}$ is the planar electromechanical coupling coefficient.

Applying the integral operator $\int_{-h/2}^{h/2} \dots dz$ to the equilibrium equations. (1a)–(1c), and using Eqs. (9a)–(9c) and (11), the governing equation of the transverse vibration is obtained as the form

$$D'\nabla^4 W - \rho h \omega^2 W = 0, \tag{12}$$

where ∇^4 is a biharmonic operator and the equivalent bending stiffness is defined by

$$D' = \frac{h^3}{12} \cdot \frac{2 - (1 - \nu_p)k_p^2}{2s_{11}^E(1 - \nu_p^2)(1 - k_p^2)}. \tag{13}$$

According to Eq. (12), the general solutions of non-axisymmetric transverse vibration for the piezoceramic annular plate is

$$W(r, \theta) = [C_1^{(n)}J_n(\beta r) + C_2^{(n)}Y_n(\beta r) + C_3^{(n)}I_n(\beta r) + C_4^{(n)}K_n(\beta r)] \cos n\theta, \quad n = 0, 1, 2, 3, \dots \tag{14a}$$

in which $C_1^{(n)} - C_4^{(n)}$ are constants and

$$\beta^4 = \frac{\rho h \omega^2}{D'} = \frac{12\rho\omega^2}{h^2} \cdot \frac{2s_{11}^E(1 - \nu_p^2)(1 - k_p^2)}{2 - (1 - \nu_p)k_p^2}. \tag{14b}$$

In Eq. (14a), J_n and Y_n are the Bessel functions of the first and second kinds, as well as I_n and K_n are the modified Bessel functions of the first and second kinds, respectively. Under consideration of the different boundary conditions on the inner and outer surfaces, four types of piezoceramic annular plates will be investigated in this analysis. For the purpose of description, a notation will be adopted that the symbolism free–fixed, for example, will identify an annulus with the inner and outer circumferences having free and fixed boundary conditions, respectively. It is noted that the theoretical model can be performed for the case of a piezoceramic circular plate and which is the same as [9].

(1) *The free–free boundary condition.* For the circumferential free boundary conditions at $r = R_i$ and R_o , we have

$$\int_{-h/2}^{h/2} z\sigma_{rr} dz = 0 \tag{15a}$$

and

$$\int_{-h/2}^{h/2} \sigma_{rz} dz + \frac{1}{r} \frac{\partial}{\partial \theta} \int_{-h/2}^{h/2} z\sigma_{r\theta} dz = 0 \tag{15b}$$

From Eqs. (15a) and (15b), a system of linear equations is obtained as

$$[A] \cdot [C] = [F], \tag{16}$$

where $[C] = [C_1^{(n)}, C_2^{(n)}, C_3^{(n)}, C_4^{(n)}]^T$, $[A]$ is a fourth-order square matrix and $[F]$ is a 4×1 zero matrix. The matrix elements of $[A]$ are

$$\begin{aligned}
 A_{11} &= G\alpha\xi \cdot J_{n+1}(\alpha\xi) + [Gn(n-1) - H(\alpha\xi)^2] \cdot J_n(\alpha\xi) \\
 A_{12} &= G\alpha\xi \cdot Y_{n+1}(\alpha\xi) + [Gn(n-1) - H(\alpha\xi)^2] \cdot Y_n(\alpha\xi) \\
 A_{13} &= -G\alpha\xi \cdot I_{n+1}(\alpha\xi) + [Gn(n-1) + H(\alpha\xi)^2] \cdot I_n(\alpha\xi) \\
 A_{14} &= G\alpha\xi \cdot K_{n+1}(\alpha\xi) + [Gn(n-1) + H(\alpha\xi)^2] \cdot K_n(\alpha\xi) \\
 A_{21} &= [H(\alpha\xi)^3 + G\alpha\xi n^2] \cdot J_{n+1}(\alpha\xi) - [H(\alpha\xi)^2 n + Gn^2(n-1)] \cdot J_n(\alpha\xi) \\
 A_{22} &= [H(\alpha\xi)^3 + G\alpha\xi n^2] \cdot Y_{n+1}(\alpha\xi) - [H(\alpha\xi)^2 n + Gn^2(n-1)] \cdot Y_n(\alpha\xi) \\
 A_{23} &= [H(\alpha\xi)^3 - G\alpha\xi n^2] \cdot I_{n+1}(\alpha\xi) + [H(\alpha\xi)^2 n - Gn^2(n-1)] \cdot I_n(\alpha\xi) \\
 A_{24} &= [-H(\alpha\xi)^3 + G\alpha\xi n^2] \cdot K_{n+1}(\alpha\xi) + [H(\alpha\xi)^2 n - Gn^2(n-1)] \cdot K_n(\alpha\xi) \\
 A_{31} &= G\xi \cdot J_{n+1}(\xi) + [Gn(n-1) - H\xi^2] \cdot J_n(\xi) \\
 A_{32} &= G\xi \cdot Y_{n+1}(\xi) + [Gn(n-1) - H\xi^2] \cdot Y_n(\xi) \\
 A_{33} &= -G\xi \cdot I_{n+1}(\xi) + [Gn(n-1) + H\xi^2] \cdot I_n(\xi) \\
 A_{34} &= G\xi \cdot K_{n+1}(\xi) + [Gn(n-1) + H\xi^2] \cdot K_n(\xi) \\
 A_{41} &= [H\xi^3 + G\xi n^2] \cdot J_{n+1}(\xi) - [H\xi^2 n + Gn^2(n-1)] \cdot J_n(\xi) \\
 A_{42} &= [H\xi^3 + G\xi n^2] \cdot Y_{n+1}(\xi) - [H\xi^2 n + Gn^2(n-1)] \cdot Y_n(\xi) \\
 A_{43} &= [H\xi^3 - G\xi n^2] \cdot I_{n+1}(\xi) + [H\xi^2 n - Gn^2(n-1)] \cdot I_n(\xi) \\
 A_{44} &= [-H\xi^3 + G\xi n^2] \cdot K_{n+1}(\xi) + [H\xi^2 n - Gn^2(n-1)] \cdot K_n(\xi)
 \end{aligned}$$

in which

$$H = \frac{1}{1 + \nu_p} + \frac{k_p^2}{2(1 - k_p^2)}, \quad G = \frac{1 - \nu_p}{1 + \nu_p}, \quad \alpha = \frac{R_i}{R_o} \quad \text{and} \quad \xi = \beta R_o. \tag{17}$$

To obtain a non-trivial solution for the constants $C_1^{(n)} - C_4^{(n)}$, the determinant of coefficient matrix $[A]$ must be equal to zero and that will yield the characteristic equation of resonant frequencies for transverse vibrations as

$$\det[A] = 0 \tag{18}$$

It should be noted that the value n in Eq. (18) refers to the number of nodal diameters, and the sequence of roots represents the number of nodal circles. From Eqs. (14b), (17) and (18), we can obtain the expression of transverse resonant frequencies for piezoceramic annular plates with circumferentially free boundary conditions

$$f = \frac{\xi^2 h}{2\pi R_o^2} \sqrt{\frac{2 - (1 - \nu_p)k_p^2}{24\rho s_{11}^E(1 - \nu_p^2)(1 - k_p^2)}} \tag{19}$$

Upon utilization of Eq. (6d), the electrical current I can be expressed as

$$\begin{aligned}
 I &= \frac{\partial}{\partial t} \int \int_S D_z \, ds \\
 &= i\omega \int_0^{2\pi} \int_{R_i}^{R_o} \left\{ \frac{d_{31}(1+v_p)z}{s_{11}^E(1-v_p^2)} \left[\frac{\partial^2 W}{\partial r^2} + \frac{1}{r} \frac{\partial W}{\partial r} + \frac{1}{r^2} \frac{\partial^2 W}{\partial \theta^2} \right] + \left[\varepsilon_{33}^T - \frac{2d_{31}^2}{s_{11}^E(1-v_p^2)} \right] E_z \right\} r \, dr \, d\theta \\
 &= i\omega \frac{2\pi V \varepsilon_{33}^T (k_p^2 - 1)}{h} \cdot R_o^2 (1 - \alpha^2). \tag{20}
 \end{aligned}$$

It is shown clearly from Eq. (20) that the electrical current I does not approach to infinity even if the transverse vibrations are excited at resonant frequencies. This implies that the resonant frequencies of transverse vibrations can not be measured by the impedance variation method, such as an impedance analyzer.

(2) *The fixed-fixed boundary condition.* For the circumferential fixed boundary conditions at $r = R_i$ and R_o , we have

$$W = 0 \tag{21a}$$

and

$$\frac{\partial W}{\partial r} = 0. \tag{21b}$$

As the similar procedure, we also obtain the fourth-order coefficient matrix $[A]$ and the elements of which are

$$\begin{aligned}
 A_{11} &= J_n(\alpha\xi), & A_{12} &= Y_n(\alpha\xi), & A_{13} &= I_n(\alpha\xi), & A_{14} &= K_n(\alpha\xi), \\
 A_{21} &= -\alpha\xi J_{n+1}(\alpha\xi) + nJ_n(\alpha\xi), & A_{22} &= -\alpha\xi Y_{n+1}(\alpha\xi) + nY_n(\alpha\xi), \\
 A_{23} &= \alpha\xi I_{n+1}(\alpha\xi) + nI_n(\alpha\xi), & A_{24} &= -\alpha\xi K_{n+1}(\alpha\xi) + nK_n(\alpha\xi), \\
 A_{31} &= J_n(\xi), & A_{32} &= Y_n(\xi), & A_{33} &= I_n(\xi), & A_{34} &= K_n(\xi), \\
 A_{41} &= -\xi J_{n+1}(\xi) + nJ_n(\xi), & A_{42} &= -\xi Y_{n+1}(\xi) + nY_n(\xi), \\
 A_{43} &= \xi I_{n+1}(\xi) + nI_n(\xi), & A_{44} &= -\xi K_{n+1}(\xi) + nK_n(\xi).
 \end{aligned}$$

By equating the determinant of $[A]$ to zero, the characteristic equation of resonant frequencies is obtained. With the aid of Eq. (19), the resonant frequencies are calculated for piezoceramic annular plates with the fixed-fixed boundary conditions. In accordance with hypothesis (d) that D_z is a constant with respect to plate thickness, the expression of the electrical current I for the fixed-fixed boundary condition is the same as Eq. (20).

(3) *The free-fixed and fixed-free boundary conditions.* By properly abstracting the elements of coefficient matrices from both situations (1) and (2) mentioned above, we could easily obtain the characteristic equations and resonant frequencies for the free-fixed and fixed-free boundary conditions. The derivation is suppressed and only the numerical results are presented in the next section.

3. Theoretical and experimental results

From the solutions for characteristic equations of resonant frequencies, the dependence of frequency parameter (ξ) on inner-to-outer radius ratios (α) is discussed. The results as shown in Figs. 2–5 are the first six transverse vibration modes for the four types of boundary conditions. In these figures, the frequency parameter square (ξ^2) is plotted as the ordinate to exhibit the variations in resonant frequencies properly. For the free–free boundary condition shown in Fig. 2, it is found that the resonant frequencies of modes 2, 4, and 6 will approach infinity when the ratio α increases, while those of modes 1, 3, and 5 are finite values. For simplicity, the vibration modes are classified into two groups, namely, Group I and Group II. When the ratio α increases from zero to one, the resonant frequency of Group I will reach a maximum and then gradually decrease to a minimum at $\alpha = 1$. For Group II, the resonant frequency reaches a minimum and increases rapidly to infinity as $\alpha \rightarrow 1$. Nevertheless, the resonant frequency variations in the fixed–fixed boundary condition show nearly the same trend and with the minimum value at $\alpha = 0$ as shown in Fig. 3. Obviously, the frequency variation tendency is neither Group I nor II and will be referred to as Group III. To know the particular features for Groups II and III, it is necessary to recognize the characteristics of mode shapes at resonance. For the annulus with the fixed boundary or the mode shape including nodal circles, the resonant frequency will increase rapidly and approach infinity for $\alpha \rightarrow 1$. On the other hand, the mode shapes of Group I, which consist of nodal diameters only, will degenerate into the nodal points for $\alpha \rightarrow 1$ as is expected. According to the classifications, the frequency variations of the free–fixed and fixed–free boundary conditions, as shown in Figs. 4 and 5, are recognized as Groups II and III, respectively. Moreover, Fig. 5 reveals that there is almost no difference among the first three modes for the fixed–free boundary

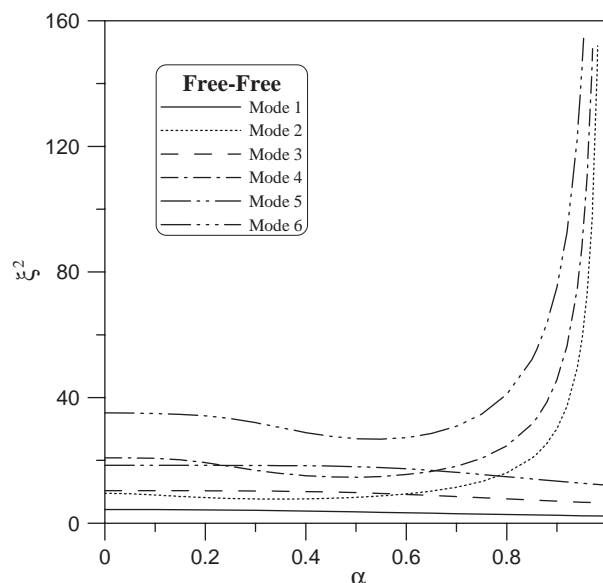


Fig. 2. The variation of frequency parameter with different α values for the free–free boundary condition.

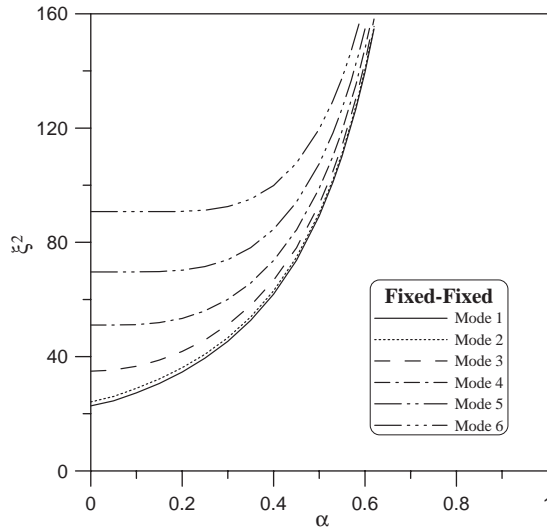


Fig. 3. The variation of frequency parameter with different α values for the fixed–fixed boundary condition.

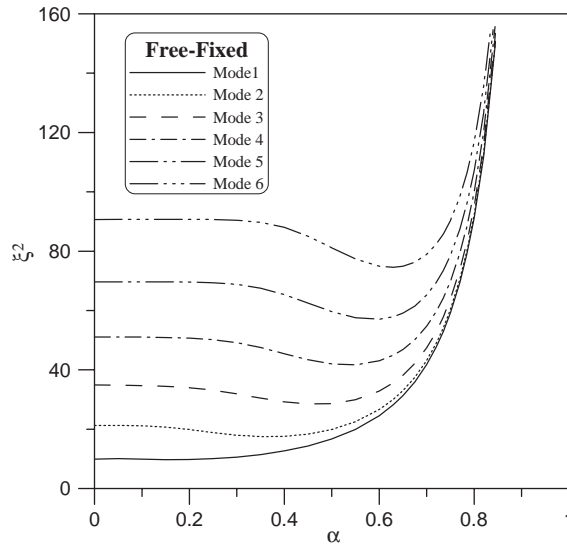


Fig. 4. The variation of frequency parameter with different α values for the free–fixed boundary condition.

conditions. This phenomenon also occurs in the case of fixed–fixed boundary conditions for the first two modes.

As a verification example, the piezoceramic annulus with $R_o = 15$ mm, $R_i = 7.5$ mm, and $h = 1$ mm is selected for experimental investigations and the modal number of which is PIC-151

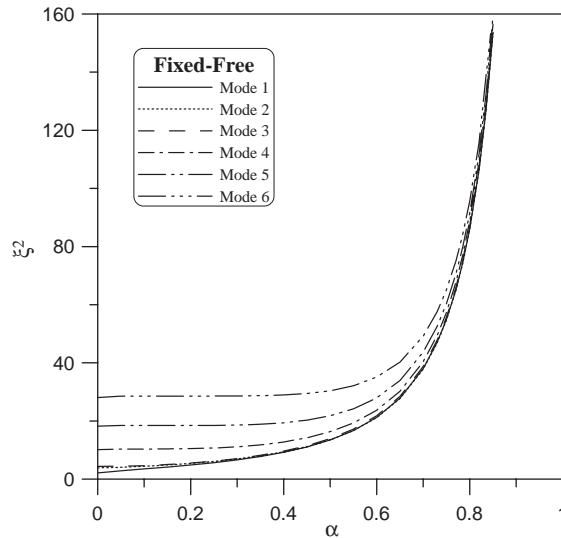


Fig. 5. The variation of frequency parameter with different α values for the fixed–free boundary condition.

Table 1
Material properties of piezoceramics PIC-151

PIC-151 Ceramics	
s_{11}^E (10^{-12} m ² /N)	16.83
s_{33}^E	19.0
s_{12}^E	−5.656
s_{13}^E	−7.107
s_{44}^E	50.96
s_{66}^E	44.97
d_{31} (10^{-10} m/V)	−2.14
d_{33}	4.23
d_{15}	6.1
ϵ_{11}^T (10^{-9} F/m)	17.134
ϵ_{33}^T	18.665
ρ (kg/m ³)	7800

(Germany Physik Instrument Company). The polarization is in the z -direction as shown in Fig. 1 and two opposite faces of the specimen are completely coated with silver electrodes. The electroelastic properties of PIC-151 piezoceramics are listed in Table 1. Table 2(a)–(d) shows the theoretical and finite element method (FEM) results for the first six transverse vibration modes of the four different boundary conditions. These results, including the resonant frequencies and mode shapes, are all calculated for the inner-to-outer radius ratio $\alpha = 0.5$. To recognize the mode shapes in Table 2, the symbol n and s illustrate the number of nodal diameters and nodal circles,

Table 2

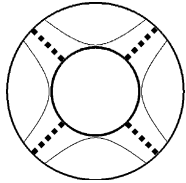
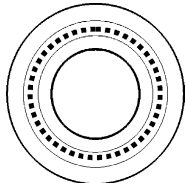
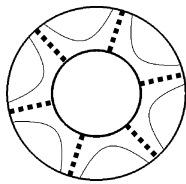
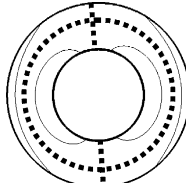
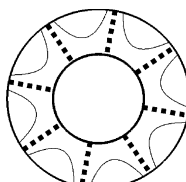
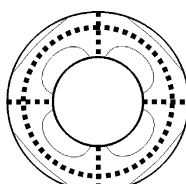
Mode number	Mode shape	(a) Theory (Hz)	(b) FEM (Hz)	(c) LDV (Hz)	Error (a)/(b) (%)
(a) Results of resonant frequencies obtained by theory, FEM, and LDV for the free-free boundary condition					
1 ($n = 2, s = 0$)		2665	2629	2508	1.37
2 ($n = 0, s = 1$)		6089	6028	5891	1.01
3 ($n = 3, s = 0$)		7169	7040	6732	1.83
4 ($n = 1, s = 1$)		10 816	10 282	10 047	5.19
5 ($n = 4, s = 0$)		13 282	12 936	12 438	2.67
6 ($n = 2, s = 1$)		19 878	18 666	18 073	6.49

Table 2 (continued)

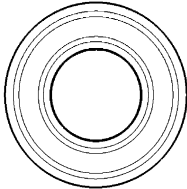
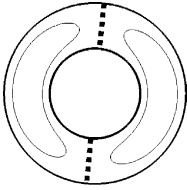
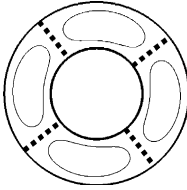
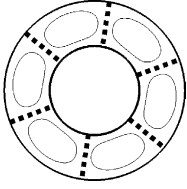
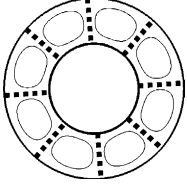
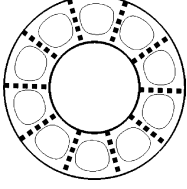
Mode number	Mode shape	Theory (Hz)	FEM (Hz)	Error (a)/(b) (%)
(b) Results of resonant frequencies obtained by theory and FEM for the fixed–fixed boundary condition				
1 ($n = 0, s = 0$)		65 913	58 756	12.18
2 ($n = 1, s = 0$)		66 636	59 306	12.36
3 ($n = 2, s = 0$)		68 919	61 079	12.84
4 ($n = 3, s = 0$)		73 060	64 394	13.46
5 ($n = 4, s = 0$)		79 440	69 638	14.08
6 ($n = 5, s = 0$)		88 398	77 105	14.65

Table 2 (continued)

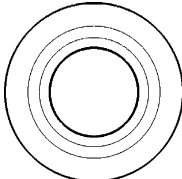
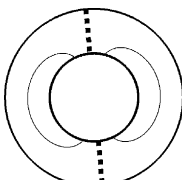
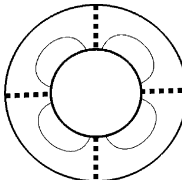
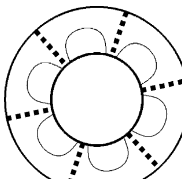
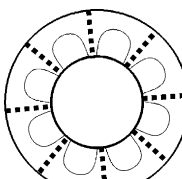
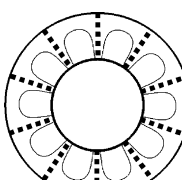
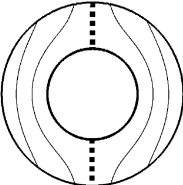
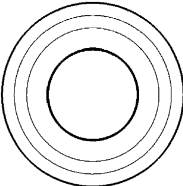
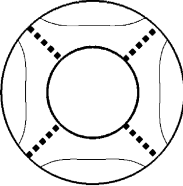
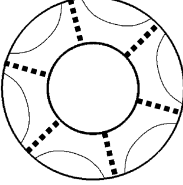
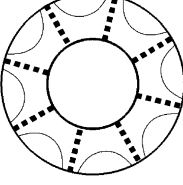
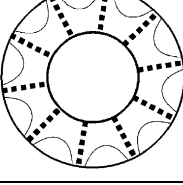
Mode number	Mode shape	Theory (Hz)	FEM (Hz)	Error (%)
(c) Results of resonant frequencies obtained by theory and FEM for the free-fixed boundary condition				
1 ($n = 0, s = 0$)		12 320	12 182	1.13
2 ($n = 1, s = 0$)		14 699	14 249	3.16
3 ($n = 2, s = 0$)		21 159	20 050	5.53
4 ($n = 3, s = 0$)		31 009	29 049	6.75
5 ($n = 4, s = 0$)		44 009	40 867	7.69
6 ($n = 5, s = 0$)		59 922	55 057	8.84

Table 2 (continued)

Mode number	Mode shape	Theory (Hz)	FEM (Hz)	Error (%)
(d) Results of resonant frequencies obtained by theory and FEM for the fixed-free boundary condition				
1 ($n = 1, s = 0$)		9977	9796	1.85
2 ($n = 0, s = 0$)		9946	9865	0.82
3 ($n = 2, s = 0$)		10 279	10 012	2.67
4 ($n = 3, s = 0$)		12 046	11 606	3.79
5 ($n = 4, s = 0$)		16 090	15 424	4.32
6 ($n = 5, s = 0$)		22 441	21 433	4.70

respectively. For example, the value $s = 0$ shown in Table 2(a)–(d) represents that no nodal circle is present between the inner and outer circumferences. It is also indicated that the order of mode shapes is not permanent and may be changed in light of different values of α . Whenever the curves of frequency parameter intersect at certain α value, the order of these two modes exchange with each other. The finite element calculation is performed by the commercially available software ABAQUS finite element package [13] in which 20-node three-dimensional solid piezoelectric elements (C3D20E) are selected to analyze the problem. The electrical potential on the surfaces $z = \pm h/2$ is specified to “zero” for simulation the closed-circuit condition in order for the resonant frequency extraction. As seen in Table 2, the error will increase not only for the higher modes, but also vary with the boundary conditions. The thickness of the piezoceramic annulus also shows significant difference between the theoretical and numerical results, because the Kirchhoff–Love plate hypotheses and three-dimensional element simulations are employed for theory and FEM, respectively.

The resonant frequency of a piezoceramic material is conventionally measured by an impedance analysis, because the electrical impedance of which will drop to a local minimum at resonance. Using an HP4194A impedance/gain-phase analyzer (Hewlett Packard), we perform the experimental impedance analysis of the piezoceramic annular plate with the free–free boundary condition. To simulate the free–free boundary, the piezoceramic annular plate is supported on a soft sponge. The local minimum and maximum appearing in the impedance variation curve correspond to the resonant and anti-resonant frequencies, respectively. Both the experimental and FEM results are available in Fig. 6. According to Eq. (20), the transverse vibration modes can not

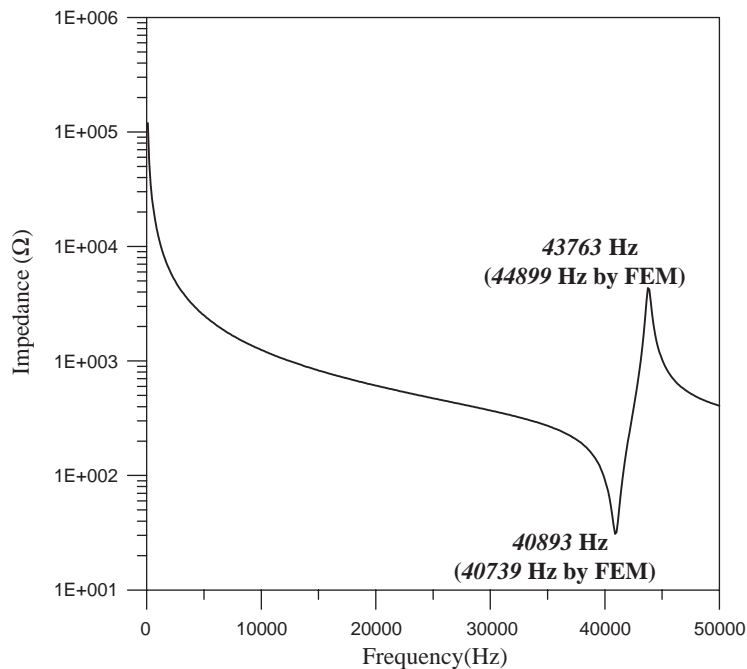


Fig. 6. Experimental impedance variation curve of the piezoceramic annular plate.

be obtained by impedance analysis and, in fact, only the first extensional vibration mode is indicated in Fig. 6. This phenomenon can be explained qualitatively by means of the characteristics of piezoelectricity. When the piezoceramic plate vibrates at a resonant frequency, the charge will greatly be induced on the electrode surfaces owing to the vibration deformation, named the direct piezoelectric effect, and the impedance will drop to a local minimum value. However, if the summation of the induced charge distributed over the electrode surfaces is zero, we are not able to find the large variation of impedance at the resonant frequency.

The other experimental technique called the laser Doppler vibrometer (LDV) is also employed to validate the transverse vibration modes, and the gain spectrum of which is shown in Fig. 7. The boundary condition configuration for LDV experiment is the same as that for impedance analysis. For the LDV system, a built-in dynamic signal analyzer (DSA) composed of dynamic signal analyzer software and a plug-in waveform generator board can provide the specimen with the swept-sine excitation signal. By the DSA calculation, the swept-sine excitation signal and the response measured by LDV are taken as input and output, respectively. After the fast Fourier transform (FFT) processing of the input and output with the DSA, the ratio of output/input (gain) is obtained. Then the resonant frequencies of transverse resonance can be obtained via peaks appearing in the frequency response curve. In Fig. 7, the first six peaks are clearly corresponding to the first six transverse resonant frequencies. The comparison of resonant frequencies obtained from the analytical method and LDV experimental measurement is in good agreement as shown in Table 2(a). This result apparently implies that only the vibration amplitude measurement can be used to obtain the transverse vibration of piezoceramic annular plates, meanwhile the impedance analysis is ineffective.

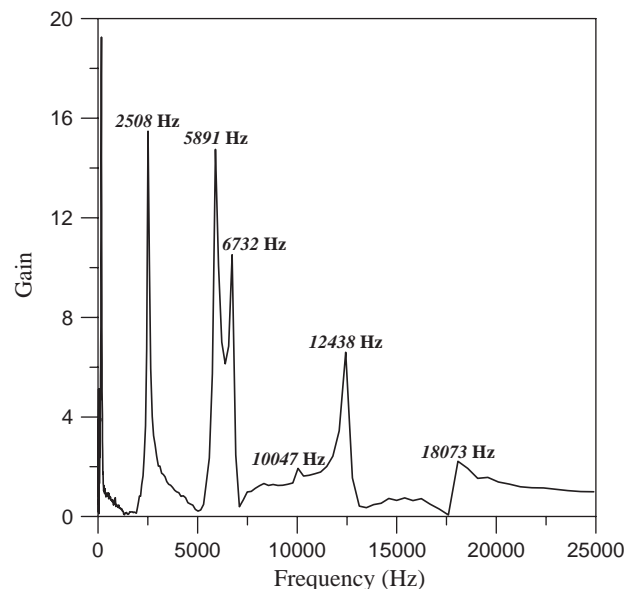


Fig. 7. LDV output gain spectrum of transverse vibrations for the piezoceramic annular plate.

4. Conclusions

The majority of the previous works on vibration investigation of piezoceramic annular plates are analytical and numerical results for in-plane (tangential or radial extensional) modes. There are very few articles available for the out-of-plane (transverse) modes of vibrating piezoceramic annuli. In this study, the transverse vibration characteristics of piezoceramic annular plates with four different boundary conditions are explored in details. The piezoceramic plate with crystal symmetry class C_{6mm} , can be indeed served as the transverse isotropic plate for flexural resonance. Consequently, both the non-axisymmetric and axisymmetric modes will be present in the analytical and experimental investigations. The resonant frequencies of transverse vibrations, which are much lower than those of in-plane vibrations, are an important factor in the transducer design and application. By the two experimental techniques, the impedance and LDV measurements, it is shown that only the resonant frequencies of radial extensional vibration can be measured by the impedance analysis, and that the existence of transverse vibrations can be verified by using the LDV techniques. Good agreement of the resonant frequencies is obtained for experimental measurements and theoretical predictions. With reference to the variation in resonant frequencies, the transverse vibration modes are classified into three groups (Groups I, II, and III). The features of Group II and III are that the resonant frequency will approach infinity as $\alpha \rightarrow 1$ when the corresponding mode shape includes the nodal circle or the annulus is with the fixed boundary. On the contrary, the resonant frequencies of Group I vibration modes are finite and the corresponding mode shapes will degenerate into the nodal points for $\alpha \rightarrow 1$.

Acknowledgements

The authors gratefully acknowledge the financial support of this research by the National Science Council (Republic of China) under Grant NSC 91-2212-E-231-002.

References

- [1] N.F. Ivina, Numerical analysis of the normal modes of circular piezoelectric plates of finite dimensions, *Soviet Physics. Acoustics* 35 (1990) 385–388.
- [2] H.A. Kunkel, S. Locke, B. Pikeroen, Finite-element analysis of vibrational modes in piezoelectric ceramics disks, *IEEE Transactions on Ultrasonics, Ferroelectrics, and Frequency Control* 37 (1990) 316–328.
- [3] N. Guo, P. Cawley, D. Hitchings, The finite element analysis of the vibration characteristics of piezoelectric discs, *Journal of Sound and Vibration* 159 (1992) 115–138.
- [4] A. Iula, N. Lamberti, M. Pappalardo, A model for the theoretical characterization of thin piezoceramic rings, *IEEE Transactions on Ultrasonics, Ferroelectrics, and Frequency Control* 43 (1996) 370–375.
- [5] A. Iula, N. Lamberti, R. Carotenuto, M. Pappalardo, Analysis of the radial symmetrical modes of thin piezoceramic rings, *IEEE Transactions on Ultrasonics, Ferroelectrics, and Frequency Control* 46 (1999) 1047–1049.
- [6] L. Shuyu, Thickness shearing vibration of the tangentially polarized piezoelectric ceramic thin circular ring, *The Journal of the Acoustical Society of America* 107 (2000) 2487–2492.
- [7] T. Takano, H. Hirata, Y. Tomikawa, Analysis of nonaxisymmetric vibration mode piezoelectric annular plate and its application to an ultrasonic motor, *IEEE Transactions on Ultrasonics, Ferroelectrics, and Frequency Control* 37 (1990) 558–565.

- [8] Q. Wang, S.T. Quek, C.T. Sun, X. Liu, Analysis of piezoelectric coupled circular plate, *Smart Materials and Structures* 10 (2001) 229–239.
- [9] C.H. Huang, C.C. Ma, Y.C. Lin, Theoretical analysis and experimental measurement for resonant vibration of piezoceramic circular plates, *IEEE Transactions on Ultrasonics, Ferroelectrics and Frequency Control* 51 (2003) 12–24.
- [10] N.N. Rogacheva, *The Theory of Piezoelectric Shells and Plates*, CRC Press, Boca Raton, FL, 1994.
- [11] H.F. Tiersten, *Linear Piezoelectric Plate Vibrations*, Plenum Press, New York, 1969.
- [12] ANSI-IEEE Std. 176, IEEE standard on piezoelectricity, The Institute of Electrical and Electronics Engineers, Inc., New York, 1987.
- [13] ABAQUS User's Manual, Version 6.3, Hibbitt, Karlsson and Sorensen, Inc., Rhode Island, 2002.